Available online at www.sciencedirect.com
ScienceDirect
Journal of Solid State Chemistry 181 (2008) 406–414
JOURNAL OF SOLID STATE CHEMISTRY
www.elsevier.com/locate/jssc

Pyrochlore formation, phase relations, and properties in the $CaO–TiO_2–(Nb,Ta)_2O_5$ systems

R.S. Roth[a], T.A. Vanderah[a,*], P. Bordet[b], I.E. Grey[c], W.G. Mumme[c], L. Cai[d], J.C. Nino[d]

[a]*Materials Science and Engineering Laboratory, National Institute of Standards and Technology, Gaithersburg, MD 20899, USA*
[b]*CNRS Laboratoire de Cristallographie, BP 166, 38042 Grenoble, France*
[c]*CSIRO Minerals, Box 312, Clayton South, Vic. 3169, Australia*
[d]*Department of Materials Science and Engineering, University of Florida, Gainesville, FL 32611-6400, USA*

Received 16 August 2007; received in revised form 29 November 2007; accepted 1 December 2007
Available online 15 December 2007

Abstract

Phase equilibria studies of the $CaO:TiO_2:Nb_2O_5$ system confirmed the formation of six ternary phases: pyrochlore ($A_2B_2O_6O'$), and five members of the (110) perovskite-slab series $Ca_n(Ti,Nb)_nO_{3n+2}$, with $n = 4.5$, 5, 6, 7, and 8. Relations in the quasibinary $Ca_2Nb_2O_7$–$CaTiO_3$ system, which contains the $Ca_n(Ti,Nb)_nO_{3n+2}$ phases, were determined in detail. $CaTiO_3$ forms solid solutions with $Ca_2Nb_2O_7$ as well as $CaNb_2O_6$, resulting in a triangular single-phase perovskite region with corners $CaTiO_3$–$70Ca_2Ti_2O_6$:$30Ca_2Nb_2O_7$–$80CaTiO_3$:$20CaNb_2O_6$. A pyrochlore solid solution forms approximately along a line from 42.7:42.7:14.6 to 42.2:40.8:17.0 $CaO:TiO_2:Nb_2O_5$, suggesting formulas ranging from $Ca_{1.48}Ti_{1.48}Nb_{1.02}O_7$ to $Ca_{1.41}Ti_{1.37}Nb_{1.14}O_7$ (assuming filled oxygen sites), respectively. Several compositions in the $CaO:TiO_2:Ta_2O_5$ system were equilibrated to check its similarity to the niobia system in the pyrochlore region, which was confirmed. Structural refinements of the pyrochlores $Ca_{1.46}Ti_{1.38}Nb_{1.11}O_7$ and $Ca_{1.51}Ti_{1.32}V_{0.04}Ta_{1.10}O_7$ using single-crystal X-ray diffraction data are reported (*Fd3m* (#227), $a = 10.2301(2)$ Å (Nb), $a = 10.2383(2)$ Å (Ta)), with Ti mixing on the A-type Ca sites as well as the octahedral B-type sites. Identical displacive disorder was found for the niobate and tantalate pyrochlores: Ca occupies the ideal 16*d* position, but Ti is displaced 0.7 Å to partially occupy a ring of six 96*g* sites, thereby reducing its coordination number from eight to five (distorted trigonal bipyramidal). The O′ oxygens in both pyrochlores were displaced 0.48 Å from the ideal 8*b* position to a tetrahedral cluster of 32*e* sites. The refinement results also suggested that some of the Ti in the A-type positions may occupy distorted tetrahedra, as observed in some zirconolite-type phases. The Ca–Ti–(Nb,Ta)–O pyrochlores both exhibited dielectric relaxation similar to that observed for some Bi-containing pyrochlores, which also exhibit displacively disordered crystal structures. Observation of dielectric relaxation in the Ca–Ti–(Nb,Ta)–O pyrochlores suggests that it arises from the displacive disorder and not from the presence of polarizable lone-pair cations such as Bi^{3+}.

Keywords: Ca–Ti–Nb–O; $CaO:TiO_2:Nb_2O_5$; Phase diagram; Pyrochlore; Crystal structure; Dielectric relaxation

1. Introduction

Ceramic dielectric materials based on complex titanates, niobates, and tantalates are important for a variety of components in communication systems [1–6]. In addition, these systems have received considerable attention for photocatalytic materials capable of splitting water [7]. The present study of the $CaO–TiO_2–(Nb,Ta)_2O_5$ systems was undertaken to clarify the equilibrium phase relationships, especially those involving ternary compounds. Studies of the $CaO:TiO_2:Ta_2O_5$ system have not been reported, to the best of our knowledge. Available information on the $CaO:TiO_2:Nb_2O_5$ system is limited to the study of Jongejan and Wilkins [8], which included work on phase relations both above and below the subsolidus. The formation of "at least two ternary compounds" was reported, a pyrochlore-type phase at $3CaO:3TiO_2:Nb_2O_5$ ($= Ca_{1.5}Ti_{1.5}NbO_7$), and other phases near 1:1:1 and 8:7:6 $CaO:TiO_2:Nb_2O_5$ which were associated with liquids. The 8:7:6 composition was reported to melt congruently at 1472 °C and exhibit a distinct X-ray powder diffraction pattern. A $CaTiO_3$ solid

*Corresponding author. Fax: +1 301 975 5334.
E-mail address: terrell.vanderah@nist.gov (T.A. Vanderah).

0022-4596/$ - see front matter © 2007 Elsevier Inc. All rights reserved.
doi:10.1016/j.jssc.2007.12.005

solution formed along the $CaTiO_3$–$CaNb_2O_6$ join, and changes in the X-ray powder diffraction pattern of $Ca_2Nb_2O_7$ were observed when $CaTiO_3$ was added along the $Ca_2Nb_2O_7$–$CaTiO_3$ composition line. The stoichiometry of $Ca_{1.5}Ti_{1.5}NbO_7$ reported for the pyrochlore [$^{VIII}A_2^{VI}B_2O_6O'$] phase drew our interest, as this would require 0.5 mol of the smaller B-type octahedral cations to mix on the (6+2)-coordinated sites of the larger A-type cations. This behavior has been observed in a number of pyrochlore systems [9] which exhibit static displacive disorder in the A_2O' sub-network that facilitates reduced coordination numbers for resident B-type cations; however, for these systems the A-type majority cations have all been lone-pair or d^{10} species such as Bi^{3+}, Tl^{+}, Sn^{2+}, Pb^{2+} or Cd^{2+}. The presence of these large, highly polarizable cations has been associated with the occurrence of the static displacive disorder [10], which in turn has been linked to unusual dielectric properties, including high relative permittivities [11] and relaxation behavior [12–15]. A key objective of the present work was to characterize the stoichiometry and dielectric properties of pyrochlores in the CaO–TiO_2–$(Nb,Ta)_2O_5$ systems.

2. Experimental methods

Approximately 30 polycrystalline specimens (3–4*g* each) were prepared in air by solid-state reactions of mixtures of $CaCO_3$ (99.99%), TiO_2 (phosphate-free), and Nb_2O_5 (99.9985%) or Ta_2O_5 (99.993%). Prior to each heating, each sample was mixed by grinding with an agate mortar and pestle for 15 min, pelletized, and placed on a bed of same-composition sacrificial powder supported on platinum foil placed on alumina ceramic. After an initial overnight calcination at 950 °C, multiple 1–7*d* heatings (with intermediate grinding and re-pelletizing) were carried out at temperatures ranging from 1300 to 1650 °C. Samples were either furnace-cooled to ≈700 °C and air-quenched on the bench-top, or quenched from high temperature into liquid nitrogen. Equilibrium was presumed when no further changes could be detected in the weakest peaks observed in the X-ray powder diffraction patterns.

Pyrochlore-type crystals in the CaO–TiO_2–Nb_2O_5 system were obtained from partial melts of the respective (equilibrated) molar compositions 34.00:45.00:21.00 (reported to occur in the pyrochlore's primary phase field [8]) and 41.67:41.67:16.67 in welded Pt capsules. Heating the first composition at 1375 °C for 143 h (followed by cooling at 200°/h to 700 °C) produced a sample that was approximately half melted and contained large crystals, some of which were euhedral octahedra. The second composition was heated at 1400 °C for 112 h (followed by cooling at 200°/h to 700 °C), showed some melting, and yielded small cubic pyrochlore crystals in addition to rutile and $CaNb_2O_6$ as impurity phases. Small single crystals from this experiment were used for the structural study. Pyrochlore-type single crystals in the CaO–TiO_2–Ta_2O_5 system were grown using a 3.000CaO:2.554V_2O_5 flux, prepared by melting the respective mixture of $CaCO_3$ and V_2O_5 at 950 °C for 2 h, and then pouring the liquid onto a chill plate. The pre-heated (@ 1300 °C for 94 h) composition 42.50:42.50:15.00 CaO–TiO_2–Ta_2O_5 was used as the charge. Greenish pyrochlore crystals were grown from both 4:1 and 1:1 (by mass) charge:flux mixtures, which were heated in Pt capsules (crimped but not welded shut) at 1425 °C for 1 h, cooled at 3 °C/h to 960 °C, and then air-quenched. After removing the flux with dilute (~3 *M*) hydrochloric acid, the 4:1 mixture yielded pyrochlore crystals as well as black rutile crystals, as did the 1:1 growth mixture, which in addition contained yellow $CaTa_2O_6$ crystals. Small crystals from the 4:1 product were selected for the structural study.

Crystals of both pyrochlores were analyzed using a JEOL electron probe microanalyzer model JXA 8900R, operated at 20 kV and 20 nA with 40 s counts on peaks and 20 s counts on backgrounds on either side. Standards used were TiO_2, V metal, Ta_2O_5 and $Ca_3Nb_2O_8$. The averages from 11 analyses on two crystals of the niobate, expressed as oxides, are 24.1 wt% CaO, 32.5 wt% TiO_2 and 43.3 wt% Nb_2O_5. The corresponding formula scaled to seven oxygen atoms is $Ca_{1.46}Ti_{1.38}Nb_{1.11}O_7$. For the tantalate, the averages from 24 analyses on four crystals are 19.5 wt% CaO, 24.4 wt% TiO_2, 55.9 wt% Ta_2O_5 and 0.84 wt% V_2O_5. The small amount of vanadium is due to incorporation from the calcium vanadate flux. The formula scaled to seven oxygen atoms is $Ca_{1.51}Ti_{1.32}V_{0.04}Ta_{1.10}O_7$.

Phase assemblages were ascertained using the disappearing phase method [16,17] and X-ray powder diffraction data obtained with a Philips [18] diffractometer equipped with incident Soller slits, a theta-compensating slit and graphite monochromator, and a scintillation detector. Samples were mounted in welled glass slides. Diffraction patterns were collected at ambient temperature using Cu $K\alpha$ radiation over the range 3–70° 2θ with a 0.02° 2θ step size and a 2 s count time. Intensity data measured as relative peak heights above background were obtained using the DATASCAN software package, and processed using JADE [19]. Single pyrochlore-type crystals were characterized by the precession camera method (Zr-filtered Mo $K\alpha$ radiation) to assess quality, cell parameter, and space group. Single-crystal intensity data were collected using Nonius Kappa CCD diffractometers (at CNRS Grenoble for the Ca–Ti–Ta–O pyrochlore and at Monash University, Clayton for the Ca–Ti–Nb–O pyrochlore).

Dielectric properties of the Ca–Ti–Nb–O pyrochlore were measured using a disk (≈6 mm in diameter, 1.5 mm thick) of pressed equilibrated powder, composition 42.50:42.50:15.00 CaO–TiO_2–Nb_2O_5, which was sintered at 1300 °C for 42 h. Density was determined geometrically. The specimen was then polished to obtain planar surfaces and gold electrodes (≈75 nm thick) were sputtered onto the pellet surfaces to form parallel plate capacitors. The capacitance and dielectric loss were measured using an Agilent 4284 LCR meter at frequencies varying from 1 kHz to 1 MHz. The reported permittivity data were corrected to

theoretical density using the Maxwell mixture equation. Sample temperature was varied between 110 and 475 K using a programmable 9023 Delta Design controller. Typical uncertainties in the permittivity data are on the order of 5% and are dominated by the geometric estimates of porosity.

3. Results and discussion

3.1. Phase equilibrium relationships

Results obtained for the $CaO:TiO_2:Nb_2O_5$ system above 50 mol% CaO are shown in Fig. 1. Only the $Ca_2Nb_2O_7$–$CaNb_2O_6$–$CaTiO_3$ section was determined in detail, as shown. The quasibinary system $Ca_4Nb_2O_9$–$CaTiO_3$ was previously studied using X-ray diffraction and transmission electron microscopy [20]; perovskite-based solid solutions $Ca[Ca_xNb_yTi_z]O_3$ form which differ in the ordering patterns of the B-type cations and the type of octahedral tilting. In the present study, specimens prepared along a composition line between perovskite-related $Ca_3Nb_2O_8$ [21] and $CaTiO_3$ exhibited no sign of solid solution formation; rather, the X-ray powder diffraction patterns suggested that the phases associated with the $Ca_4Nb_2O_9$–$CaTiO_3$ system are in equilibrium with those along the $Ca_2Nb_2O_7$–$CaTiO_3$ line; the details were not investigated further.

Phase relations determined along the line $Ca_2Nb_2O_7$–$CaTiO_3$ are illustrated in Figs. 1 and 2. A homologous series $Ca_n(Ti,Nb)_nO_{3n+2}$ forms, with $n=4.5$, 5, 6, 7, and 8, as also observed in the $Sr_n(Ti,Nb)_nO_{3n+2}$ system [22]. The family members adopt structures composed of

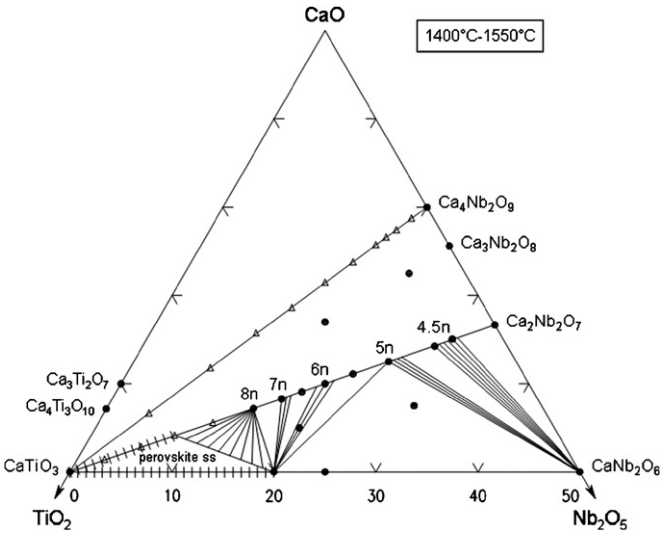

Fig. 1. Phase equilibrium relations in the $CaO:TiO_2:Nb_2O_5$ system above 50 mol% CaO; closed circles indicate the compositions prepared. The region above the $CaTiO_3$–$Ca_2Nb_2O_7$ line was not studied in detail, except to determine that a join between $Ca_3Nb_2O_8$ does not exist. A homologous series $Ca_n(Ti,Nb)_nO_{3n+2}$ forms, with $n=4.5$, 5, 6, 7, and 8. $CaTiO_3$ solid solutions form along lines toward $Ca_2Nb_2O_7$ as well as $CaNb_2O_6$, thereby delineating a triangular single-phase perovskite region with corners $CaTiO_3$–$70Ca_2Ti_2O_6$:$30Ca_2Nb_2O_7$–$80CaTiO_3$:$20CaNb_2O_6$.

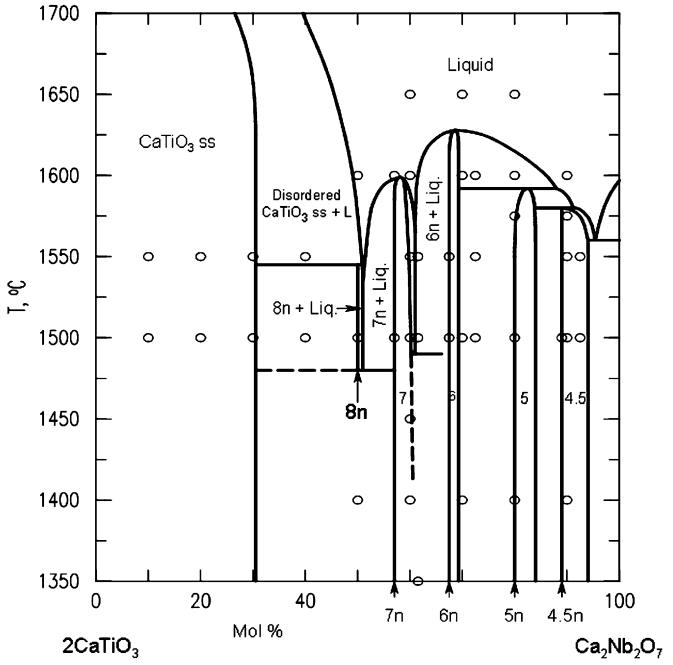

Fig. 2. Phase equilibrium relations in the quasibinary $Ca_2Nb_2O_7$–$2CaTiO_3$ system; open circles indicate the compositions prepared. The $Ca_n(Ti,Nb)_nO_{3n+2}$ homologs with $n=4.5$, 5, 6, and 7 all exhibited solid solution regions, as also indicated in Fig. 1.

slabs of the distorted perovskite structure that are n $[(Ti,Nb)O_6]$ octahedra thick and extend parallel to the $\{110\}_{\text{cubic perovskite}}$ planes. For the $n=4.5$ member, the slabs are alternately four- and five-octahedra in width. For the end-member $Ca_2Nb_2O_7$, $n=4$ ($Ca_4Nb_4O_{14}$). The phases in this series have in common a basic orthorhombic sub-cell with $a\approx a_{\text{perovskite}}$, $c\approx\sqrt{2}a_{\text{perovskite}}$, and a long b-axis that increases systematically with increasing slab thickness (n-value). The actual structures are determined by the superposition of a variety of effects on the basic sub-cell, including translation of the slabs and octahedral tilting, which can result in superstructures, reduced symmetry, and/or modulated structures [23–26]. For the $Ca_n(Ti,Nb)_nO_{3n+2}$ system, the $n=4.5$, 5, and 6 members were previously reported by Nanot et al. [23,24]; however, the present study found that the $n=7$ and 8 members also form. Analysis of the X-ray powder diffraction patterns for the $n=7$ and 8 phases indicated orthorhombic sub-cells consistent with those reported for the lower n-values [23,24] (i.e. $a\approx3.83$ Å, $c\approx5.45$ Å, and $b\approx42.66$ Å ($n=7$); 48.13 Å ($n=8$)); however, the actual structures were not characterized further. The low-angle regions of the X-ray powder diffraction patterns which reveal the characteristic $(0k0)$ reflections for the different homologs are shown in Fig. 3. As indicated in Figs. 1 and 2, the $n=4.5$, 5, 6, and 7 members all exhibited solid solution regions along the $Ca_2Nb_2O_7$–$CaTiO_3$ composition line; the phase relations found in this quasibinary system are shown in detail in Fig. 2.

$CaTiO_3$ was found to dissolve $Ca_2Nb_2O_7$ up to the composition $70Ca_2Ti_2O_6$:$30Ca_2Nb_2O_7$, with a gradually

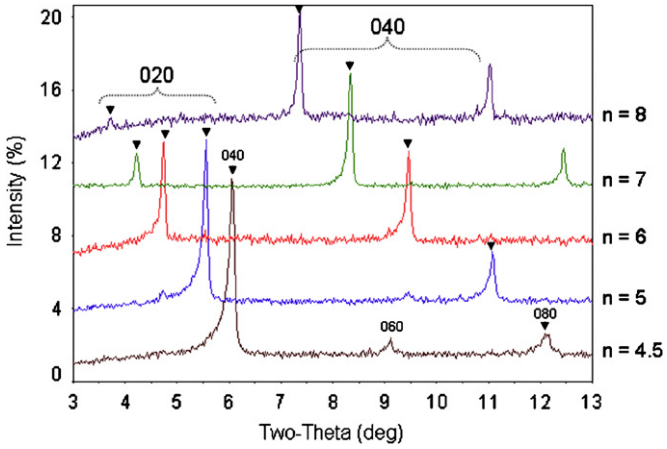

Fig. 3. Low-angle X-ray powder diffraction patterns for the homologous series $Ca_n(Ti,Nb)_nO_{3n+2}$ with $n = 4.5$, 5, 6, 7, and 8. The characteristic $0k0$ reflections reveal the systematic increase in the b parameter of the orthorhombic sub-cell with increasing n-value or thickness of the distorted perovskite slabs, whereas the a and c parameters of the family members are similar. The 0 2 0 and 0 4 0 reflections are indicated with triangles for each homolog. (For the $n = 4.5$ phase, the b parameter and the corresponding k indices are doubled because of the alternation of $n = 4$ and 5 slabs.)

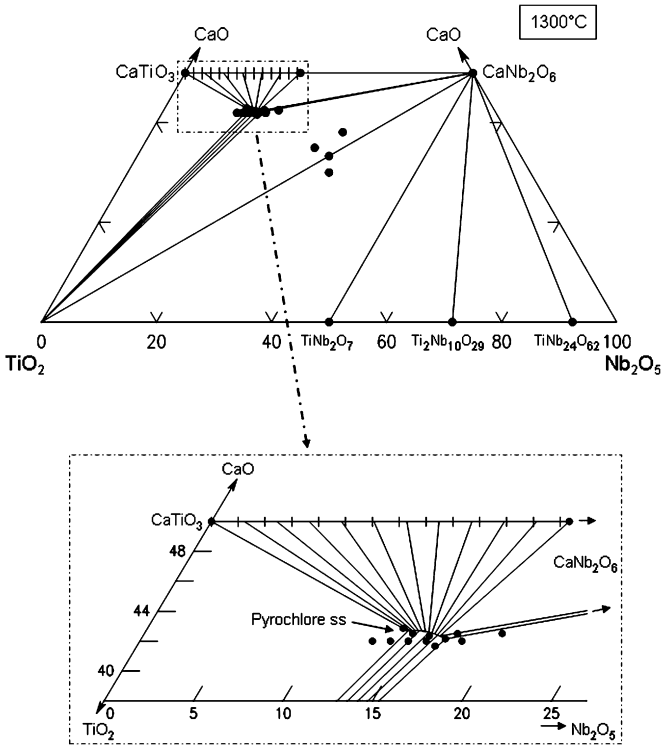

Fig. 4. Phase equilibrium relations in the $CaO:TiO_2:Nb_2O_5$ system below 50 mol% CaO; closed circles indicate the compositions prepared. The only ternary compound found was a pyrochlore phase which formed a solid solution ranging from 42.7:42.7:14.6 to 42.2:40.8:17.0 $CaO:TiO_2:Nb_2O_5$, suggesting that ≈ 0.5 mol Ti^{4+} mixes on the A-type sites with Ca^{2+}. Normalized to seven oxygens, the pyrochlore formulas ranged from $Ca_{1.48}Ti_{1.48}Nb_{1.02}O_7$ to $Ca_{1.41}Ti_{1.37}Nb_{1.14}O_7$.

increasing unit cell volume. Consistent with the earlier work [8], $CaTiO_3$ also dissolved up to 20 mol% $CaNb_2O_6$, with a gradually increasing unit cell volume. These solid solutions therefore form two sides of a triangular single-phase perovskite region with corners $CaTiO_3$–$70Ca_2Ti_2O_6$:$30Ca_2Nb_2O_7$–$80CaTiO_3$:$20CaNb_2O_6$ (Fig. 1).

Subsolidus phase equilibrium relations in the $CaO:TiO_2:Nb_2O_5$ system below 50 mol% CaO are shown in Fig. 4. The only ternary compound found was the pyrochlore phase; specimens prepared at and near 1:1:1 and 8:7:6 $CaO:TiO_2:Nb_2O_5$ were mixtures confirming a $CaNb_2O_6$–TiO_2 join and a $CaNb_2O_6$–TiO_2–pyrochlore compatibility triangle, respectively. When these specimens were heated at higher temperatures ($\geqslant 1350\,^{\circ}C$) producing liquid, however, quenched specimens were mixtures with some X-ray powder diffraction peaks matching those reported by Jongejan and Wilkens [8] for the "8:7:6" phase. The results of the present study, which included several crystal-growth experiments at temperatures from 1350 to 1500 °C, suggest that the 1:1:1 and 8:7:6 phases correspond to a single metastable quenched liquid and are not equilibrium phases.

The detailed inset in Fig. 4 shows the region of formation of the pyrochlore structure, which melted incongruently between 1325 and 1350 °C. Pyrochlore forms a solid solution approximately along a line with endpoints 42.7:42.7:14.6 and 42.2:40.8:17.0 $CaO:TiO_2:Nb_2O_5$, suggesting formulas ranging from $Ca_{1.48}Ti_{1.48}Nb_{1.02}O_7$ to $Ca_{1.41}Ti_{1.37}Nb_{1.14}O_7$ (assuming full occupancy of the oxygen sites). This compositional range suggests that ≈ 0.5 mol Ti^{4+} mixes on the A sites with Ca^{2+}, and that low levels (on the order of a few percent) of vacancies occur on the A- and/or oxygen sites. Careful heating of the stoichiometric $3CaO:3TiO_2:Nb_2O_5$ ($= Ca_{1.5}Ti_{1.5}NbO_7$) specimen resulted in pyrochlore and a small amount of $CaTiO_3$; therefore, this composition is close to but slightly outside the single-phase region. As shown in Fig. 4, the pyrochlore phase forms equilibrium mixtures with the $CaTiO_3$–$CaNb_2O_6$ solid solution, TiO_2, and $CaNb_2O_6$.

A small number of compositions in the $CaO:TiO_2:Ta_2O_5$ system were prepared to check its similarity to the niobia system, particularly in the region of pyrochlore formation. Analogous to the Nb_2O_5 system, a join was found between $CaTa_2O_6$ and TiO_2. The pyrochlore phase formed in a composition region similar to that found for niobia, with the stoichiometric point $3CaO:3TiO_2:Ta_2O_5$ ($= Ca_{1.5}Ti_{1.5}TaO_7$) similarly occurring slightly outside the single-phase region. The Ta-pyrochlore analogously forms equilibrium mixtures with $CaTiO_3$ (and its solid solution), $CaTa_2O_6$, and TiO_2. The Ta_2O_5 system was more refractory, as expected, with synthesis and subsolidus temperatures $\approx 100\,^{\circ}C$ higher than those in the Nb_2O_5 system.

3.2. Structural refinements of the Ca–Ti–(Nb,Ta)–O pyrochlores

Precession photographs obtained for single crystals of the Ca–Ti–Nb–O and Ca–Ti–Ta–O pyrochlores exhibited

weak forbidden reflections (e.g., 442) indicative of displacements off the ideal crystallographic positions for this structure-type [9]. Full structural refinements were carried out to characterize the details of the displacements. The crystal data and data collection parameters are summarized in Table 1. The structural refinements were initiated in *Fd3m* (second setting) using ideal pyrochlore coordinates, with *M*(1) in 16*c* (0,0,0); *M*(2) in 16*d* (1/2,1/2,1/2); O(1) in 48*f* (*x*,1/8,1/8) with $x = 0.33$; and O(2) in 8*b* (3/8,3/8,3/8). The stoichiometries obtained from the microprobe analyses were assumed in the refinements. All the Nb or Ta was placed in the *M*(1) sites which were then filled with Ti; the remaining Ti and Ca were assigned to the A-type *M*(2) sites. The occupancy factors for the oxygen sites were assumed to be 1.0.

Refinement of the data for $Ca_{1.51}Ti_{1.32}V_{0.04}Ta_{1.10}O_7$ using isotropic displacement parameters converged at $R_1 = 0.076$ for 228 observed reflections. The displacement parameter for O(2) was unreasonably large ($U = 0.1$ Å^2) and a difference Fourier map showed a tetrahedral cluster of peaks around the O(2) site at (*x*,*x*,*x*), $x = 0.40$. The largest peaks in the difference Fourier map (6 e/Å^3) were clustered around the ideal *M*(2) (1/2,1/2,1/2) site, at 0.47,0.47,0.55, corresponding to the 96*g* position (*x*,*x*,*z*). By analogy with other pyrochlore structures containing small cations in the *M*(2) site [14], these peaks were interpreted as being due to a relocation of the Ti atom to achieve satisfactory coordination and meet its valence requirements. With the Ti(2) and O(2) atoms located to the displaced positions, an isotropic refinement converged at $R_1 = 0.040$. A difference Fourier map showed that the main residual electron density was located close to O(1) and *M*(1). The atomic displacement parameters for these two atoms, as well as the Ca(2) atom at 1/2,1/2,1/2 were refined anisotropically, resulting in convergence at $R_1 = 0.025$ for the observed reflections and 0.039 for all 356 unique reflections.

The same refinement procedure was followed for $Ca_{1.46}Ti_{1.38}Nb_{1.11}O_7$. Almost identical displacements of disordered O(2) and Ti(2) atoms were found for this phase as for the tantalate. A final refinement with isotropic displacement parameters for the disordered Ti(2) and O(2) atoms and anisotropic parameters for *M*(1), Ca(2) and O(1) converged at $R_1 = 0.037$ for the observed reflections and 0.063 for all 342 unique reflections. The refined parameters for both phases are reported in Table 2.

In the pyrochlore structure, composition $M(2)_2M(1)_2O(1)_6O(2)$, small *M*(1) atoms form an octahedral framework of composition $M(1)_2O(1)_6$. This network comprises interconnected {111} layers of corner-shared octahedra that form three- and six-member rings in a hexagonal tungsten bronze (HTB) configuration. The larger *M*(2) atoms occupy the centers of the hexagonal rings and coordinate to a further two oxygen atoms, O(2), located above and below the rings, giving hexagonal bipyramidal coordination. In the case of the Ca–Ti–Nb–O

Table 1
Summary of crystal data, collection, and refinement conditions for Ca–Ti–(Nb,Ta)–O pyrochlores

	$Ca_{1.46}Ti_{1.38}Nb_{1.11}O_7$	$Ca_{1.51}Ti_{1.32}V_{0.04}Ta_{1.10}O_7$
Crystal data		
Space group	*Fd3m* (no. 227)	*Fd3m*
Unit cell parameter (Å)	10.2301 (2)	10.2383 (2)
Volume (Å^3)	1070.6	1073.2
Z	8	8
Molecular weight	339.69	436.78
Calculated density (g/cm^3)	4.21	5.40
Crystal size	Plate, $0.15 \times 0.15 \times 0.05$ mm^3	Octahedron, center-to-face = 0.08 mm
Absorption coefficient (mm^{-1})	5.76	13.74
Data collection		
Collection mode	Nonius Kappa CCD. ϕ scan 0–360°, 1° steps $+5 \times \Omega$ scans, 60 s/frame	
Wavelength	Mo $K\alpha$	Ag $K\alpha$
2θ max (°)	107.6	79.8
Total no. reflections	18,511	6.274
No. of unique reflections	342	356
No. of reflections, $F > 4\sigma(F)$	226	278
Absorption correction	Multi-scan (SADABS) $T_{min}/T_{max} = 0.7$	Multi-scan (SORTAV) $T_{min} = 0.10$, $T_{max} = 0.23$
R (int)	0.064	0.065
Refinement		
No. of parameters refined	16	16
R_1, $F > 4\sigma(F)$	0.037	0.025
R_1, all reflections	0.063	0.039
wR_2, all reflections	0.119	0.069
Max residual electron density	1.7 e/Å^3, 0.35 Å from Ti(2)	1.9 e/Å^3, 0.37 Å from Ti(2)

Table 2
Refined coordinates and isotropic displacement parameters for Ca–Ti–(Nb,Ta)–O pyrochlores

	$Ca_{1.46}Ti_{1.38}Nb_{1.11}O_7$	$Ca_{1.51}Ti_{1.32}V_{0.04}Ta_{1.10}O_7$[a]
***M*(1)**	0.555Nb + 0.445Ti	0.550Ta + 0.450Ti
Site 16*c*	0,0,0	0,0,0
U (Å^2)	0.0155(2)	0.0098(1)
Ca(2)	0.730Ca	0.755Ca
Site 16*d*	1/2,1/2,1/2	1/2,1/2,1/2
U(Å^2)	0.0151(2)	0.0154(2)
Ti(2)	0.245/6Ti	0.230/6Ti
Site 96*g*; *x*,*x*,*z*	$x = 0.4737(5)$, $z = 0.5565(7)$	$x = 0.4738(5)$, $z = 0.5572(7)$
U (Å^2)	0.0079(8)	0.0027(7)
O(1)		
Site 48*f*; *x*,1/8,1/8	$x = 0.3237(3)$	$x = 0.3223(3)$
U (Å^2)	0.0188(4)	0.0152(4)
O(2)	0.25O	0.25O
Site 32*e*; *x*,*x*,*x*	$x = 0.4022(6)$	$x = 0.4014(7)$
U (Å^2)	0.015(1)	0.014(2)

[a]In the structural refinement the small amount of V was incorporated on the *M*(1) site and given the same scattering factor as Ti.

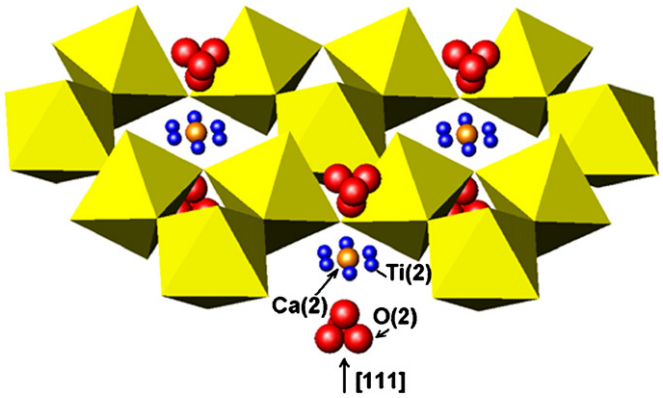

Fig. 5. Portion of an HTB layer of corner-connected $M(1)O_6$ octahedra, illustrating the displacive disorder in the $M(2)_2O(2)$ pyrochlore sub-network. The *M*(2) Ca atoms (light-colored spheres) are located centrally in the hexagonal rings, surrounded by the six partially occupied sites for Ti(2) (small dark spheres). The O(2) atoms (large dark spheres) are disordered among a tetrahedral cluster of sites above and below, along the [111] direction.

and Ca–Ti–Ta–O pyrochlore phases, the refinements are consistent with the *M*(2) site being occupied by a mixture of large Ca and small Ti atoms in the ratio ≈3Ca:Ti. The Ca atoms occupy the *M*(2) 16*d* sites at (1/2,1/2,1/2) whereas the Ti atoms are displaced from the 16*d* sites by 0.7 Å along six equivalent directions very close to $\langle 11\bar{2}\rangle$. The six fractionally occupied Ti(2) sites are at the vertices of a hexagon, normal to the three-fold axis passing through the 16*d* site, as shown in Fig. 5. The Ti(2) atoms bond to three O(1) atoms within the HTB plane, and to two O(2)

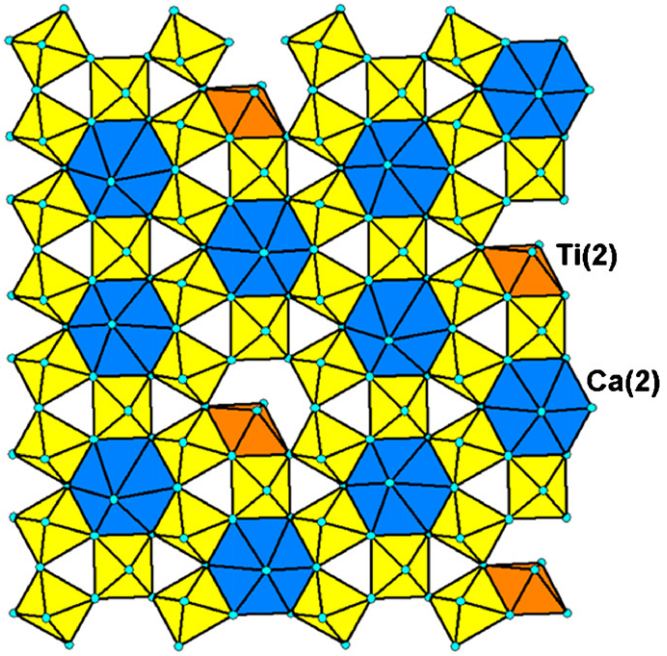

Fig. 6. Polyhedral representation of a (111) HTB layer in the Ca–Ti–(Nb,Ta)–O pyrochlores, showing a possible local ordering of $Ti(2)O_5$ trigonal prisms (medium shaded, Ti(2)) and $Ca(2)O_8$ hexagonal bipyramids (dark shaded, Ca(2)) in the six-member rings.

atoms above and below, giving trigonal bipyramidal coordination as illustrated in Fig. 6. The $Ti(2)O_5$ geometry, with three shorter bonds at 1.8–1.9 Å and two longer bonds at 2.2–2.3 Å, is the same as has been reported for small atoms such as Ti and Ta occupying sites in the hexagonal rings of HTB layers in zirconolite-type phases [27,28].

In addition to a large displacement of Ti(2) from the ideal site in $Ca_{1.46}Ti_{1.38}Nb_{1.11}O_7$ and $Ca_{1.51}Ti_{1.32}V_{0.04}Ta_{1.10}O_7$, the oxygen atom O(2) is also displaced markedly from the ideal 8*b* position at (3/8,3/8,3/8) to a 32*e* position (*x*,*x*,*x*), with $x \sim 0.401$. This corresponds to a displacement of each O(2) along $\langle 111\rangle$ directions by 0.48 Å in both phases. The disordered O(2) atoms form tetrahedral clusters, with one site on the three-fold axis passing through the adjacent *M*(2) site and the other three sites distributed around the axis as shown in Fig. 5. The O(2) on the three-fold axis bonds to Ti(2) at ≈1.9 Å, while the off-axis O(2) atoms bond to Ca at ≈2.4 Å (see Table 3). The ratio of 1:3 for the on- and off-axis O(2) atoms matches the ≈1:3 ratio of Ti(2):Ca(2).

For both pyrochlores, the structural results suggest an additional position for the Ti(2) atom. The largest residual electron density (1.7–1.9 e/Å^3) occurred at the same position for both phases, (0.5,0.54,0.46), located 0.37 Å from the 16*d* position along $\langle 1\bar{1}0\rangle$ directions. Locating Ti at this site, Ti(2A), and refining the Ti(2):Ti(2A) site occupancy factors resulted in a lowering of the agreement factors (R_1 decreased from 0.037 to 0.031 for $Ca_{1.46}Ti_{1.38}Nb_{1.11}O_7$ and from 0.025 to 0.022 for $Ca_{1.51}Ti_{1.32}V_{0.04}Ta_{1.10}O_7$), and gave a ratio of Ti(2):Ti(2A)

Table 3
Polyhedral bond lengths (Å) for Ca–Ti–(Nb,Ta)–O pyrochlores

M–O	Distance (Å)	
	$Ca_{1.46}Ti_{1.38}Nb_{1.11}O_7$	$Ca_{1.51}Ti_{1.32}V_{0.04}Ta_{1.10}O_7$
M(1)–O(1) × 6	1.959(1)	1.955(1)
Ca(2)–O(1) × 6	2.554(2)	2.567(2)
–O(2) × 2	2.418(5)	2.414(6)
Ti(2)–O(2)	1.85(1)	1.86(1)
–O(1)	1.882(2)	1.889(8)
–O(2)	1.89(1)	1.91(1)
–O(1) × 2	2.289(3)	2.299(3)

occupancies of ~4. The Ti(2A) atoms bond to two O(2) anions at 1.85 Å and to two O(1) anions at 2.05 Å, forming distorted tetrahedra. The Ti(2A)–O(1) bonds are too long for tetrahedral titanium. This is most likely an artifact of the average structure refinement, which gives only the mean position of the oxygen atoms. In the structurally related zirconolite phases, both trigonal bipramidal and tetrahedral coordination is observed for small atoms such as Ti^{4+} located within the large hexagonal rings of the HTB layers [28].

3.3. Dielectric properties of the Ca–Ti–Nb–O pyrochlore

Preliminary capacitance measurements of Ca–Ti–Nb–O and Ca–Ti–Ta–O pyrochlores [9,29] suggested that both phases exhibited dielectric relaxation resembling that observed in bismuth pyrochlores (e.g. Bi–Zn–Nb–O [12,13,30,31] and Bi–Fe–Nb–O [15]). The real and imaginary parts of the relative permittivity for a pyrochlore specimen of composition 42.50:42.50:15.00 $CaO:TiO_2:Nb_2O_5$ are shown in Fig. 7 as a function of temperature and frequency from 1 kHz to 1 MHz. (This composition lies slightly outside the single-phase pyrochlore region and contained a just-detectable amount of rutile (on the order of 1–2%)). Remarkably, a dielectric relaxation characteristic of bismuth-based pyrochlores is clearly observed [31]; that is, with increasing measuring frequency the peak of the dielectric loss shifts towards higher temperatures and the width and maximum of the dielectric loss peak increases. At 1 MHz, the Ca–Ti–Nb–O pyrochlore exhibits a maximum relative dielectric permittivity of ≈107 at 200 K, and the peak of the dielectric loss occurs at $T_m \approx 150$ K. When compared with the bismuth niobate pyrochlores, the Ca–Ti–Nb–O analog exhibits a higher T_m but a lower dielectric constant. To better understand the phenomenon, the Arrhenius function was used to model the relaxation behavior:

$$\nu = \nu_0 \exp\left[-\frac{E_a}{kT}\right],$$

where ν is the measuring frequency, the pre-exponential ν_0 is the attempt-jump frequency, E_a is the activation energy, and k_B is Boltzmann's constant. T_m was determined for each measuring frequency by fitting the peak of the imaginary part of the relative permittivity to a Gaussian function. The resulting Arrhenius plot is shown in Fig. 8. From the linear fit, $\nu_0 = 4.6 \times 10^{14}$ Hz and the activation energy E_a is 0.32 eV. Both the attempt-jump frequency and the activation energy are higher than those of Bi-based pyrochlores [30,31]. Previously, the attempt-jump frequency which drives the relaxation has been correlated with that of the O′–A–O′ bending phonon mode [13]. Since the A-site atoms in Ca–Ti–Nb–O

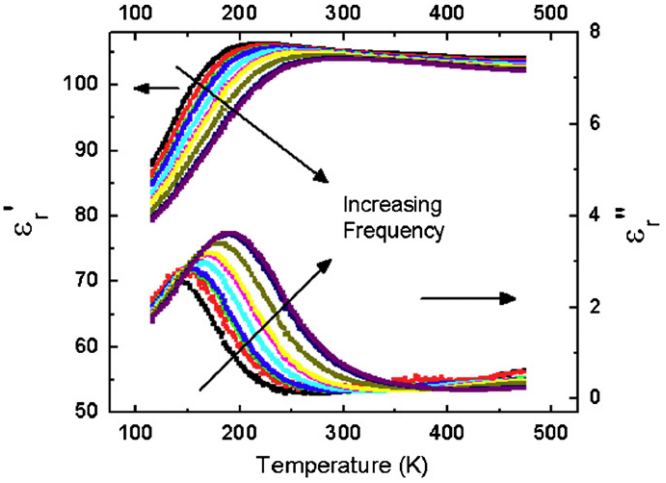

Fig. 7. Relative dielectric permittivity (ε') and dielectric loss (ε'') for a pyrochlore specimen 42.50:42.50:15.00 $CaO:TiO_2:Nb_2O_5$, measured at (from left to right) 1, 3, 8, 10, 30, 80, 100, 300, 800 kHz and 1 MHz. Below 300 K, the dielectric relaxation characteristic of bismuth based pyrochlores is clearly observed. In the temperature region above 300 K the relative permittivity is 100–105 and its temperature coefficient is slightly negative.

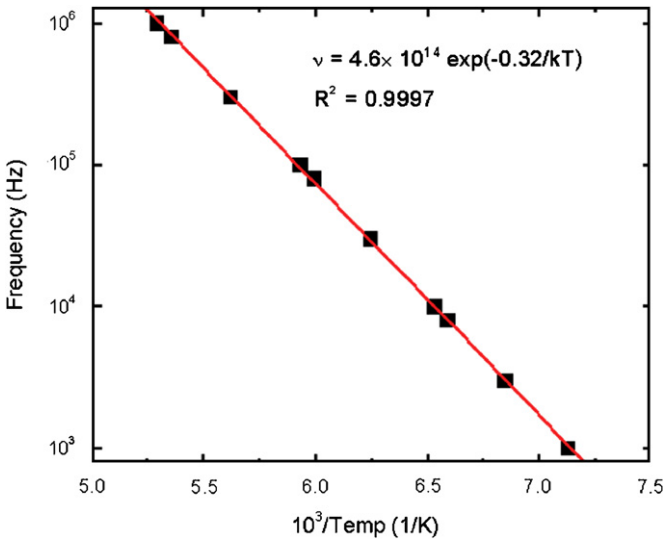

Fig. 8. Arrhenius plot of measuring frequency and T_m, the temperature at which the maximum in the dielectric loss peak occurs, for the pyrochlore specimen 42.50:42.50:15.00 $CaO:TiO_2:Nb_2O_5$. The equation for the linear least squares fit is given along with the goodness of the fit.

pyrochlore (Ca and Ti) are lighter than those in Bi-based pyrochlores (primarily Bi), higher frequencies for the O′–A–O′ bending phonon mode and the attempt-jump frequency are expected. Although the activation energy for the Ca–Ti–Nb–O pyrochlore is higher than that observed for the bismuth pyrochlores (e.g. for Bi–Zn–Nb–O, $E_a \approx 0.14$ eV), it is lower than that recently measured for weberite-type (and pyrochlore-related) $Gd_2(Gd,Nb)_2O_7$ ($E_a \approx 0.45$ eV) [32].

The Ca–Ti–(Nb,Ta)–O pyrochlores, like the bismuth analogs, exhibit substantial displacive disorder in their A_2O' sub-networks. Observation of dielectric relaxation in these systems suggests, for the first time, that it arises from the displacive disorder and is not necessarily associated with the presence of polarizable lone-pair cations such as Bi^{3+}. This observation suggests that further investigations may result in a fundamental change in the understanding and analysis of dielectric relaxation in all fluorite-related materials.

4. Conclusions

Phase equilibria studies of the $CaO:TiO_2:Nb_2O_5$ system confirmed the formation of five members of the (110) perovskite-slab series $Ca_n(Ti,Nb)_nO_{3n+2}$ ($n = 4.5$, 5, 6, 7, and 8) which form along the $CaTiO_3$–$Ca_2Nb_2O_7$ composition line; relations in this quasibinary system were determined in detail. The formation of $CaO:TiO_2:(Nb,Ta)_2O_5$ pyrochlores was also confirmed, at stoichiometries with ''excess'' Ti that mixes with Ca on the A-type sites [$^{VIII}A_2^{VI}B_2O_6O'$]. In the niobia system, pyrochlore formed a solid solution from 42.7:42.7:14.6 to 42.2:40.8:17.0 $CaO:TiO_2:Nb_2O_5$ ($= Ca_{1.48}Ti_{1.48}Nb_{1.02}O_7$ to $Ca_{1.41}Ti_{1.37}Nb_{1.14}O_7$, assuming filled O-sites), and the tantalate pyrochlore was similar. As observed for a number of bismuth-based analogs, these pyrochlores are characterized by displacive disorder in the A_2O' sub-network. Single-crystal structural refinements indicated identical displacive disorder in both systems: the A-type sites are $\approx$75% occupied by Ca^{2+} in the ideal 16*d* position and $\approx$25% by Ti^{4+}, which is displaced 0.7 Å to partially occupy a ring of six 96*g* sites and reduce its effective coordination number to 5 (trigonal bipyramidal). The O′ oxygens are disordered among a tetrahedral cluster of 32*e* sites displaced 0.48 Å from the ideal 8*b* site. The refinement results also suggested that $\approx$20% of the Ti in the A-type positions may occupy different displaced sites that result in distorted tetrahedral coordination, resulting in both five- and four-coordinated Ti^{4+} in the channels of the HTB layers, as observed in some zirconolite-type phases. The Ca–Ti–(Nb,Ta)–O pyrochlores both exhibited dielectric relaxation similar to that observed for some Bi-containing pyrochlores. Since these Bi-pyrochlores also exhibit displacively disordered crystal structures, the origin of the dielectric relaxation apparently lies in the structural disorder, not in the presence of polarizable lone-pair cations such as Bi^{3+}.

Acknowledgments

The authors appreciate the assistance of L. Cranswick in the analysis of preliminary crystallographic data, and thank N. Wilson for the microprobe analyses. J.C.N. acknowledges financial support by the US National Science Foundation (CAREER Grant, DMR-0449710) for the dielectric measurement instrumentation.

References

[1] T. Negas, G. Yeager, S. Bell, R. Amren, in: P.K. Davies, R.S. Roth (Eds.), NIST Spec. Pub. 804, US Government Printing Office, Washington, DC, 1991, pp. 21–37.
[2] W. Wersing, in: B.C.H. Steele (Ed.), Electronic Ceramics, Elsevier Applied Science, New York, 1991 Chapter 4.
[3] P.K. Davies, in: T. Negas, H. Ling (Eds.), Materials and Processes for Wireless Communications, vol. 53, The American Ceramic Society, Westerville, OH, 1995, pp. 137–151.
[4] W. Wersing, in: Current Opinion in Solid State & Materials Science, vol. 1, Current Chemistry Ltd., 1996, pp. 715–731.
[5] R.J. Cava, J. Mater. Chem. 11 (2001) 54–62.
[6] T.A. Vanderah, Science 298 (2002) 1182–1184 and references cited therein.
[7] W.G. Mumme, I.E. Grey, R.S. Roth, T.A. Vanderah, J. Solid State Chem., 2007, doi:10.1016/j.jssc.2007.06.014.
[8] A. Jongejan, A.L. Wilkins, J. Less-Common Met. 21 (1970) 225–253.
[9] T.A. Vanderah, I. Levin, M.W. Lufaso, Eur. J. Inorg. Chem. 2005 (14) (2005) 2895–2901 and references cited therein.
[10] M. Avdeev, M.K. Haas, J.D. Jorgensen, R.J. Cava, J. Solid State Chem. 169 (2002) 24–34.
[11] B. Melot, E. Rodriguez, T. Proffen, M.A. Hayward, R. Seshadri, Mater. Res. Bull. 41 (2006) 961–966.
[12] S. Kamba, V. Porokhonskyy, A. Pashkin, V. Bovtun, J. Petzelt, J.D. Nino, S. Trolier-McKinstry, M.T. Lanagan, C.A. Randall, Phys. Rev. B 66 (2002) 054106.
[13] J.C. Nino, M.T. Lanagan, C.A. Randall, S. Kamba, Appl. Phys. Lett. 81 (23) (2002) 4404–4406.
[14] I. Levin, T.G. Amos, J.C. Nino, T.A. Vanderah, C.A. Randall, M.T. Lanagan, J. Solid State Chem. 168 (2002) 69–75.
[15] M.W. Lufaso, T.A. Vanderah, I.M. Pazos, I. Levin, R.S. Roth, J.C. Nino, V. Provenzano, P.K. Schenck, J. Solid State Chem. 179 (2006) 3900–3910.
[16] C.S. Barrett, Structure of Metals, first ed., McGraw-Hill, New York, 1943 Chapter 10.
[17] C.G. Bergeron, S.H. Risbud, Introduction to Phase Equilibria in Ceramics, American Ceramic Society, Westerville, 1984.
[18] Certain commercial equipment and software are identified in order to adequately specify the experimental procedure; recommendation or endorsement by the National Institute of Standards and Technology is not therein implied.
[19] JADE + XRD Pattern Processing Software, v. 6; DATASCAN XRD Control and Acquisition Software, Materials Data Inc., Livermore, CA, 94550, www.materialsdata.com.
[20] L.A. Bendersky, I. Levin, R.S. Roth, A.J. Shapiro, J. Solid State Chem. 160 (2001) 257–271.
[21] L.M.D. Cranswick, W.G. Mumme, I.E. Grey, R.S. Roth, P. Bordet, J. Solid State Chem. 172 (2003) 178–187.
[22] I. Levin, L.A. Bendersky, T.A. Vanderah, R.S. Roth, O.M. Stafsudd, Mater. Res. Bull. 33 (3) (1998) 501–517.
[23] M. Nanot, F. Queyroux, J.-C. Gilles, J. Solid State Chem. 28 (1979) 137–147.
[24] M. Nanot, F. Queyroux, J.-C. Gilles, J. Solid State Chem. 38 (1981) 74–81.
[25] I. Levin, L.A. Bendersky, T.A. Vanderah, Phil. Mag. A 80 (2) (2000) 411–445.

[26] I. Levin, L.A. Bendersky, Acta Crystallogr. B 55 (1999) 853–866.
[27] B.M. Gatehouse, I.E. Grey, R.J. Hill, H.J. Rossell, Acta Crystallogr. B 37 (1981) 306–312.
[28] I.E. Grey, W.G. Mumme, T.J. Ness, R.S. Roth, K.L. Smith, J. Solid State Chem. 174 (2003) 285–295.
[29] P. K. Davies, unpublished data, 2002.
[30] D.P. Cann, C.A. Randall, T.R. Shrout, Solid State Commun. 100 (7) (1996) 529–534.
[31] J.C. Nino, M.T. Lanagan, C.A. Randall, J. Appl. Phys. 89 (8) (2001) 4512–4516.
[32] L. Cai, J.C. Nino, J. Eur. Ceram. Soc. 27 (2007) 3971–3976.